Dynamic Properties of Nonequilibrium Plasma in Disk MHD Generator

Y. Yoshikawa,* S. Kabashima,† H. Yamasaki,† and S. Shioda‡
Tokyo Institute of Technology, Yokohama, Japan

The realization of the stable plasma due to the fully ionized seed has been dynamically confirmed in a channel of the closed cycle disk generator by solving time-dependent MHD equations. The relaxation process is examined near the inlet of the disk generator. In the stable state, as the load resistance increases, the width of the relaxation region becomes narrower and, as a result, the uniformity of the plasma in a whole channel becomes better. The influences of the inlet conditions on changes of the relaxation region are also examined.

Nomenclature

A = energy loss due to collision
$\boldsymbol{B}$ = $(0,0,B)$ magnetic field vector
B_λ = Planck function
e = electron charge
$\boldsymbol{E}$ = $(E_r,E_\theta,0)$ electric field vector
F = plasma volume
g_i = statistical weight of the ground state of ith atom
g_i^+ = statistical weight of the ground state of ith ion
h = Planck's constant; also channel height
$\boldsymbol{j}$ = $(j_r,j_\theta,0)$ current density vector
k = Boltzmann constant
k_{fN} = ionization rate of argon
k_{fS} = ionization rate of potassium
k_{rN} = recombination rate of argon
k_{rS} = recombination rate of potassium
m_e = mass of electron
m_i = mass of ith particle
n_e = electron number density
n_{ei} = inlet electron number density
n_i = number density of ith atom
n_i^+ = number density of ith ion
p_e = electron pressure $(=n_e k T_e)$
Q_r = radiative energy loss
S = plasma surface
T_e = electron temperature
T_{eu} = uniform value of electron temperature
T_g = gas temperature
T_W = wall temperature
$\boldsymbol{u}$ = $(u_r,0,0)$ heavy species flow velocity vector
$\boldsymbol{u}_e$ = electron drift velocity
β = Hall parameter
$\Delta\lambda$ = broadening of potassium resonance line
ϵ_i = (ionization potential of ith atom)$/k$
ν_e = total collision frequency of electron
ν_{e-i} = collision frequency between electron and ith particle
σ = electrical conductivity (σ_{ideal})
σ_{eff} = effective electrical conductivity
$\sigma_W^2(T_e)$ = spatial variance around averaged T_e over the channel
$\sigma_\theta^2(T_e)$ = spatial variance around T_e of the uniform region

Subscripts

i = representing the particle
N = noble gas atom (= argon)
r,θ = coordinate direction
S = seed atom (= potassium)

Received Oct. 30, 1984; revision received April 24, 1985.

*Graduate Student, Department of Energy Sciences.
†Associate Professor, Department of Energy Sciences.
‡Professor, Department of Energy Sciences.

Introduction

IT has been shown that the reduction of power due to the ionization instability in the closed-cycle MHD power generation can be eliminated by using the concept of the fully ionized seed.[1] The results of the shock tunnel experiments performed by the group at Tokyo Institute of Technology have shown the advantage of a disk generator with fully ionized seed.[2-5]

Steady-state analyses also help ensure theoretically the high performance of the full-scale disk generator.[6,7]

It is also important to confirm the dynamic realization of the stable state due to the fully ionized seed in the MHD generator channel. The main purpose of this report is to investigate the dynamic realization of the stable plasma in a disk channel due to the fully ionized seed by numerical analysis using time-dependent MHD equations. The influence of the change of the load resistance and the inlet boundary condition are also described.

Basic Equations and Procedure of Calculation

The calculation is based on the two temperature model equations of the closed-cycle MHD plasma.[8-10] In this model the equations of MHD plasma can be written as

$$\frac{\partial n_e}{\partial t}+\nabla\cdot(n_e\boldsymbol{u}_e)=\dot{n}_e \tag{1}$$

$$\boldsymbol{j}+(\beta/B)\boldsymbol{j}\times\boldsymbol{B}=\sigma[\boldsymbol{E}^*+1/(en_e)\nabla P_e] \tag{2}$$

$$\frac{\partial U_e}{\partial t}+\nabla\cdot(U_e\boldsymbol{u}_e)=\frac{j^2}{\sigma}-A-p_e\nabla\cdot\boldsymbol{u}_e-Q_r-\nabla\cdot\boldsymbol{q}_e \tag{3}$$

where

$$\boldsymbol{E}^*=\boldsymbol{E}+\boldsymbol{u}\times\boldsymbol{B},\qquad \dot{n}_e=\dot{n}_N+\dot{n}_S$$

$$\therefore\ \dot{n}_i=k_{fi}n_e n_i-k_{ri}n_e^2 n_i^+,\qquad k_{ri}=1.09\times10^{-20}T_e^{-9/2}$$

$$\therefore\ k_{fi}=k_{ri}2(g_i/g_i^+)(2\pi m_e kT_e/h^2)^{3/2}\exp(-\epsilon_i/T_e)$$

the argon atom and potassium atom are taken as the ith particle,

$$U_e = (3/2)n_e k T_e + \epsilon_N n_N^+ + \epsilon_S n_S^+$$

$$\epsilon_N = 1.388 \times 10^5, \qquad \epsilon_S = 5.035 \times 10^4$$

$$A = 3kn_e(T_e - T_g)\sum_i \frac{m_e}{m_i}\nu_{e-i}$$

the argon atom, argon ion, potassium atom, and potassium ion are taken as the ith particle,

$$Q_r = (S/F)\pi\Delta\lambda\{B_\lambda(T_e) - B_\lambda(T_w)\}$$

$$\nabla \cdot q_e = \frac{3}{2}\frac{k}{n_e}\frac{T_e}{\nu_e}\frac{1}{1+\beta^2}\left\{\frac{1}{r}\frac{\partial}{\partial r}\left(r\frac{\partial T_e}{\partial r}\right) + \frac{1}{r^2}\frac{\partial^2 T_e}{\partial \theta^2}\right\}$$

In these equations, a two-dimensional $r-\theta$ coordinate system and magnetic field perpendicular to the disk plane are adopted, and the following assumptions are also made: charge neutrality, low magnetic field; that is, the heavy particle flow is assumed to be constant throughout the generator.

Using the above assumptions, field equations are represented by

$$\text{rot}\boldsymbol{E} = 0 \tag{4}$$

$$\text{div}\boldsymbol{j} = 0 \tag{5}$$

By integrating along the z direction, Eq. (5) is reduced to

$$\frac{\partial j_r}{\partial r} + \frac{\partial j_\theta}{r\partial\theta} = 0 \tag{6}$$

Substituting Eq. (2) into Eq. (6), we get an elliptic function,

$$\frac{\partial}{\partial r}\left\{\sigma^*\left(-\frac{\partial\phi}{\partial r}\right) - \sigma^*\beta\left(-\frac{\partial\phi}{r\partial\theta}\right) + (\sigma^* E_{nr} - \sigma^*\beta E_{n\theta}) + \sigma^*\beta u_r B\right\} + \frac{\partial}{r\partial\theta}\left\{\sigma^*\beta\left(-\frac{\partial\phi}{\partial r}\right) + \sigma^*\left(\frac{\partial\phi}{r\partial\theta}\right) + (\sigma^*\beta E_{nr} + \sigma^* E_{n\theta}) - \sigma^* u_r B\right\} = 0 \tag{7}$$

using the potential function defined as

$$E_r = -\frac{\partial\phi}{\partial r}, \qquad E_\theta = -\frac{\partial\phi}{r\partial\theta} \tag{8}$$

where

$$\sigma^* = \frac{\sigma}{1+\beta^2}, \quad E_{nr} = \frac{k}{en_e}\frac{\partial}{\partial r}(n_e T_e), \quad E_{n\theta} = \frac{k}{en_e}\frac{\partial}{r\partial\theta}(n_e T_e) \tag{9}$$

To obtain the electron temperature and the electron number density, the energy equation (3) and electron continuity equation (1) are transformed as follows,

$$\frac{\partial T_e}{\partial t} + u_r\frac{\partial T_e}{\partial r} + \left(T_e + \frac{\epsilon_N}{3/2k}\right)\frac{\dot{n}_N^+}{n_e} + \left(T_e + \frac{\epsilon_S}{3/2k}\right)\frac{\dot{n}_S^+}{n_e} = \left(\frac{j^2}{\theta} - A - p_e\nabla\cdot u - Q_r - \nabla\cdot q_e\right)/(3/2kn_e) \tag{10}$$

$$\frac{\partial n_e}{\partial t} = \dot{n}_e - u_r\frac{\partial n_e}{\partial r} \tag{11}$$

In the practical calculation, Eqs. (7), (10), and (11) are used as the basic equations instead of Eqs. (1), (2), and (3). The generator channel size is determined on the basis of the characteristic length of the plasma, which is shown in Fig. 1, where the channel of constant area of cross section is assumed. In Fig. 1, direction of magnetic field and gas velocity are also shown.

Constant electron temperature of 3500 K and three kinds of electron number densities are assumed as inlet boundary conditions. The outlet boundary condition is assumed as $(\partial T_e/\partial r)_{\text{out}} = 0$. The validity of this outlet boundary condition is obtained after calculations. We could get uniform plasma without the region near the anode. The initial electron temperature is assumed to be the same as the inlet one and a Gaussian distributed disturbance is introduced, where the standard deviation of the disturbance is given as 5 K. Here the initial and boundary values of electron temperature, 3500 K, are assumed to reduce the calculation time, but this value is not too far from a realistic situation because the plasma radiation can be observed at the region just close to the anode.[11] As the electrical boundary condition, the potential function is assumed to be 0 at the anode and cathode.

Calculations are based on the finite difference method, and the generator channel is divided into 20 mesh points along the r direction and 100 mesh points along the θ direction. One elementary section used for calculation is schematically described in Fig. 2, where the data for 9 points marked by dark circles are used in the representation of the difference equation at point N.

The time step should be chosen small enough as compared with the changes of n_e and T_e[10] and is determined up to 0.01 μs.

The initial potential distribution is obtained from Eq. (7), based on the initial and boundary conditions mentioned before.

After obtaining ϕ, T_e, and n_e distributions in the channel at $t=0$, the T_e and n_e for the next time step are obtained from Eqs. (10) and (11), and the potential ϕ is determined by Eq. (7).

Results and Discussions

Evolution Properties

Table 1 shows the conditions of the working gas, magnetic field strength, and load resistance used in these calculations. These load resistances are selected to realize the stable plasma from the quasi-one-dimensional calculation.[6]

The evolutions of average electron temperature $\langle T_e \rangle$ and electron number density $\langle n_e \rangle$ over the channel obtained from the numerical calculation for argon seeded with potassium for load resistance 3.59Ω are shown in Fig. 3, where the average electron temperature and electron number density are defined

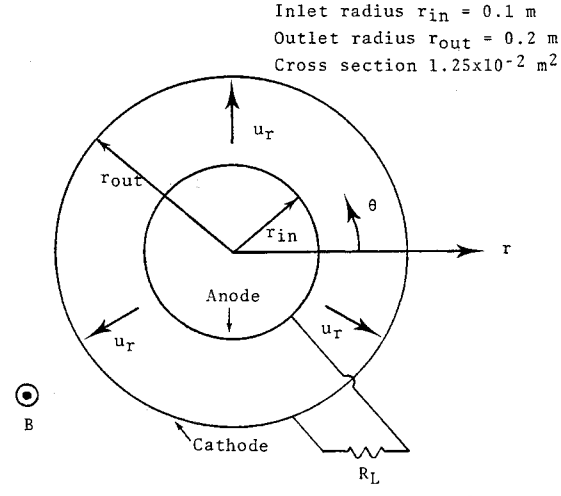

Fig. 1 Schematic of the disk generator used in the numerical calculations.

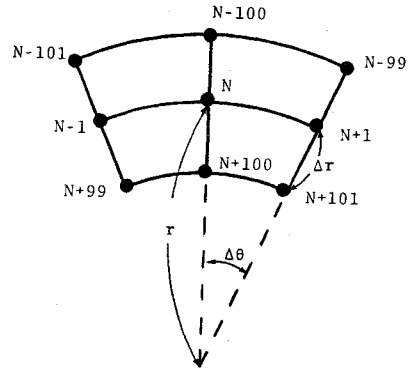

Fig. 2 Schematic view of elementary mesh section used in our calculation. The data for 9 points marked by dark circles are used for the difference equation at point N.

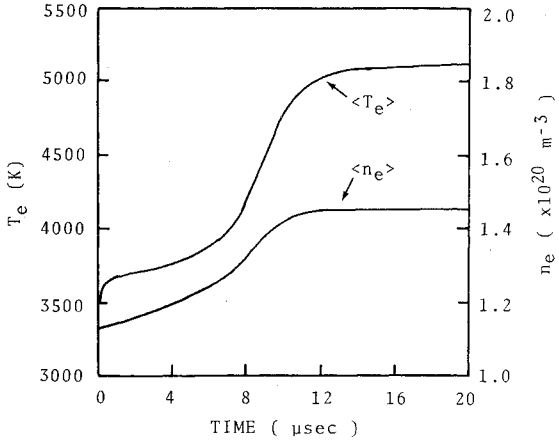

Fig. 3 Evolutions of the averaged electron temperature $\langle T_e \rangle$ and the electron number density $\langle n_e \rangle$ with time over the channel ($R_L = 3.59\Omega$).

as

$$\langle T_e \rangle = \sum_{i=1}^{N} n_e(i) T_e(i) \Big/ \sum_{i=1}^{N} n_e(i), \quad \langle n_e \rangle = \sum_{i=1}^{N} n_e(i) \Big/ N \qquad (12)$$

where $T_e(i)$ and $n_e(i)$ represent the electron temperature and electron number density at the ith mesh element, respectively, and N represents the total number of elements. It is found from this figure that $\langle T_e \rangle$ and $\langle n_e \rangle$ attain steady values at approximately 12 μs.

Figure 4 shows the temporal development of the isothermal pattern of electron temperature T_e and the current stream function inside the whole channel for the same conditions, where ψ is introduced by

$$j_r = \frac{1}{rh} \frac{\partial \psi}{\partial \theta}, \qquad j_\theta = -\frac{1}{h} \frac{\partial \psi}{\partial r} \qquad (13)$$

using the channel height h. The intervals of T_e and ψ are 500 K and 10% of total current, respectively. This figure shows that the distribution of T_e is highly disturbed at approximately 9 μs; and as the time increases, the disturbance becomes weaker except at the region near the channel inlet called the relaxation region.

The temporal development of the variance of spatial distribution of electron temperature is shown in Fig. 5, where the variance $\sigma_W^2(T_e)$ is defined as

$$\sigma_W^2(T_e) = \sum_{i=1}^{N} n_e(i) \{ T_e(i) - \langle T_e \rangle \}^2 \Big/ \sum_{i=1}^{N} n_e(i) \qquad (14)$$

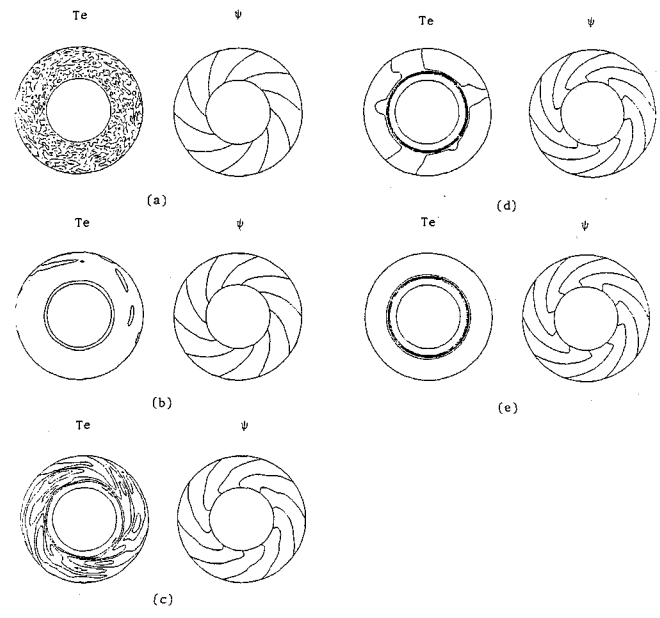

Fig. 4 Distribution of the isothermal line of T_e and current streamline for five different cases of time instances: a) 0 μs, b) 5 μs, c) 9 μs, d) 14 μs, e) 20 μs; the intervals of T_e and ψ are 500 K and 10% of the total current, respectively ($R_L = 3.59\Omega$).

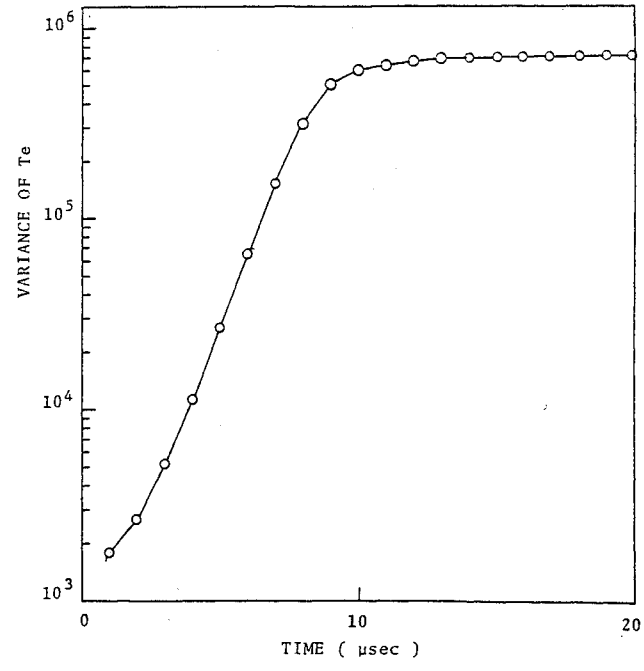

Fig. 5 Temporal development of the variance of spatial distribution of T_e ($R_L = 3.59\Omega$).

It is seen in this figure that the variance attains steady value at approximately 12 μs. From the behaviors of $\langle T_e \rangle$ and $\sigma_W^2(T_e)$, it can be confirmed that the whole plasma in the channel reaches the steady state at the end of our calculation time, even though the plasma changes locally near the inlet region.

Figure 6 shows the changes of $\langle T_e \rangle$ and $\langle n_e \rangle$ with time for several load resistances. The load resistances are considered as 3.59Ω, 3.94Ω, and 4.37Ω, and the other conditions are kept the same as listed in Table 1. It is shown for these three load resistances that as the load resistance increases, $\langle T_e \rangle$ and $\langle n_e \rangle$ rapidly reach the steady state of stable plasma.

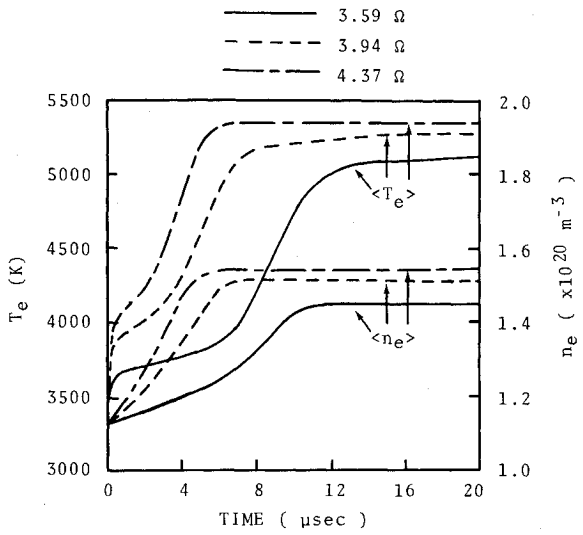

Fig. 6 Evolution of $\langle T_e \rangle$ and $\langle n_e \rangle$ with time for three kinds of load resistance.

The behavior of variance $\sigma_W^2(T_e)$ of spatial distribution of the electron temperature also supports the above results. The development of $\sigma_W^2(T_e)$ with time is shown in Fig. 7, where it is found that as the load resistance increases, $\sigma_W^2(T_e)$ reaches the steady state faster. This variance also shows the degree of inhomogeneity of the plasma in the channel. As the load resistance increases, the variance becomes smaller so that good uniformity is achieved. The reason $\sigma_W^2(T_e)$ does not approach 0 at steady state is that the relaxation region exists near the channel inlet.

The Steady-State Plasma

On the left-hand side, in Fig. 8, the distributions of the electron temperature averaged over the tangential direction $\langle T_e \rangle_\theta$ are plotted along the radial direction of the generator and, on the right-hand side, isothermal lines of T_e inside the whole channel are described at the end point of the time interval. Case a corresponds to the load resistance of 3.59Ω, case b to that of 3.94Ω, and case c to that of 4.37Ω. Near the inlet region, T_e increases from 3500 K to the uniform value in the downstream, and this region is represented as the relaxation

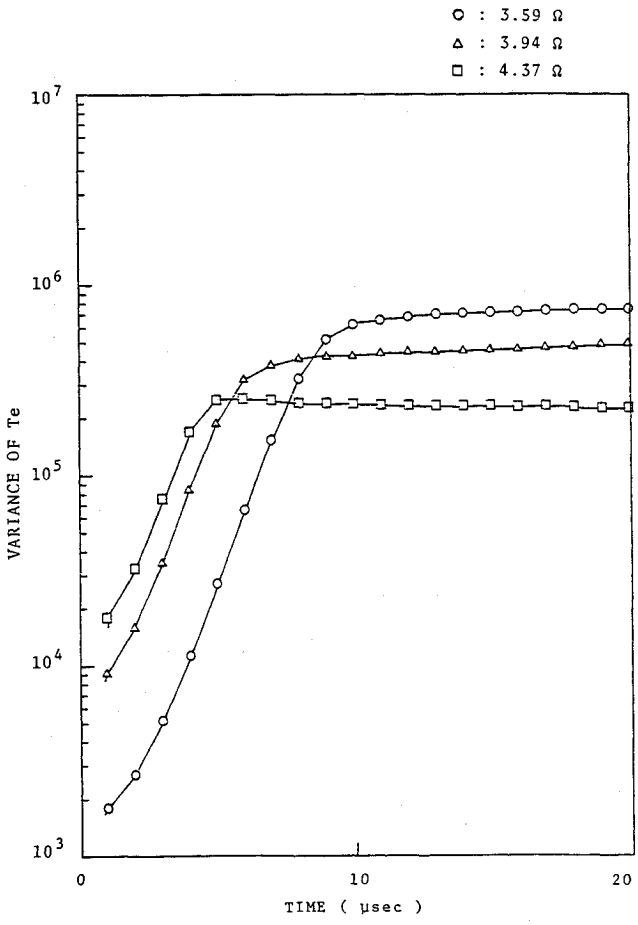

Fig. 7 Changes in the variance of spatial distribution of T_e for three kinds of load resistance.

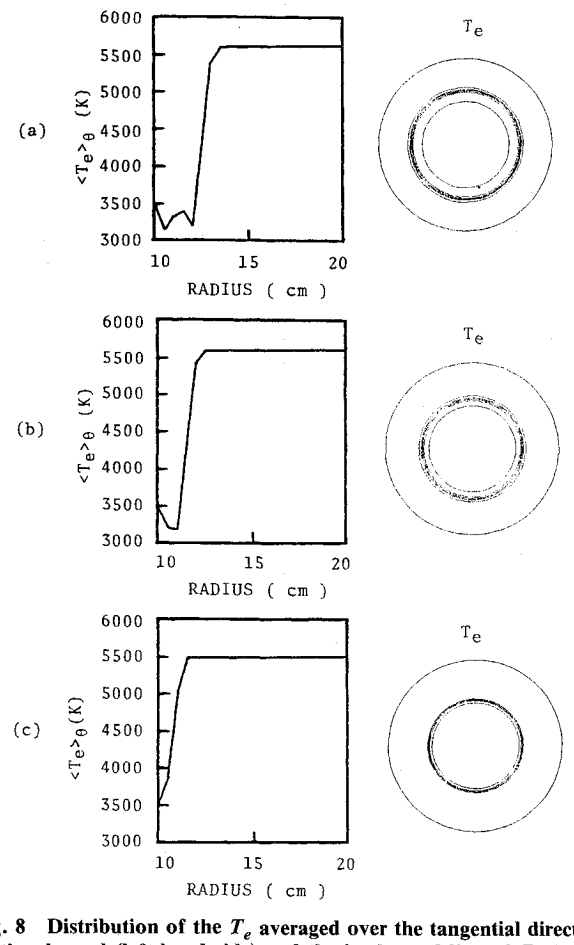

Fig. 8 Distribution of the T_e averaged over the tangential direction of the channel (left-hand side) and the isothermal line of T_e (right-hand side) for a) $R_L = 3.59\Omega$, b) $R_L = 3.94\Omega$, c) $R_L = 4.37\Omega$ (at 20 μs).

Table 1 Plasma parameters for investigating the effect of the change in load resistance

Inert gas	Seed	Stagnant pressure, atm	Stagnant temperature, K	Seed fraction, $\times 10^{-5}$	Mach number	Magnetic field strength, T	Load resistance, Ω	Inlet n_e, ×the Saha equilibrium value
Ar	K	10	2000	1.0	1.5	7.0	3.59	1
Ar	K	10	2000	1.0	1.5	7.0	3.94	1
Ar	K	10	2000	1.0	1.5	7.0	4.37	1

region. In this region the electron conductivity is low and, as a result, the tangential direction of the current stream becomes opposite to that in the case of the uniform region. The fully ionized seed is achieved in the uniform region. The broad relaxation region reduces the performance of the generator so that it is necessary to make this region narrower. From the comparison of the results for cases a, b, and c, it is shown that as the load resistance increases, the relaxation region becomes narrower.

To estimate numerically the width of the relaxation region, we consider the variance of the distribution of electron temperature for constant radius in the θ direction defined as

$$\sigma_\theta^2(T_e,r) = \sum_{i=1}^{100} n_e(r,i)\{T_e(r,i) - T_{eu}\}^2 \Big/ \sum_{i=1}^{100} n_e(r,i) \qquad (15)$$

and is plotted along the radial direction in Fig. 9. Here $T_e(r,i)$ and $n_e(r,i)$ represent the electron temperature and the electron number density at ith mesh element at radius r, respectively, and T_{eu} is the uniform value of T_e in the downstream, the summation is made in the θ direction. The distances required to get the value of $\sigma_\theta^2(T_e,r)$ nearly 0 are 3 cm for case a ($R_L = 3.59\Omega$), 2 cm for case b ($R_L = 3.94\Omega$), and 1.5 cm for case c ($R_L = 4.37\Omega$). In this figure it is clearly shown that in the steady state the width of the relaxation region becomes narrower with increasing load resistance.

Furthermore, the relation between the load resistance and the recovery factor $R_f(=\sigma_{eff}/\sigma_{ideal})$ of the electrical conductivity is examined for several load resistances and is shown in

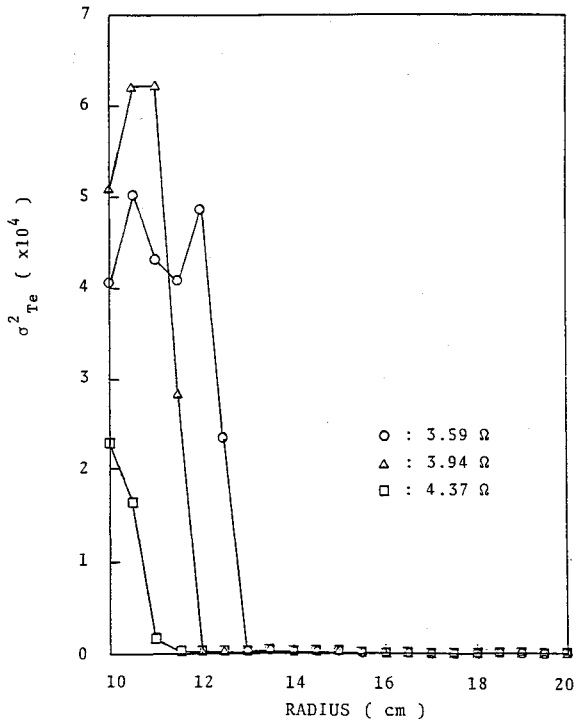

Fig. 9 The variance in the distribution of T_e for a constant radius in the θ direction (at 20 μs).

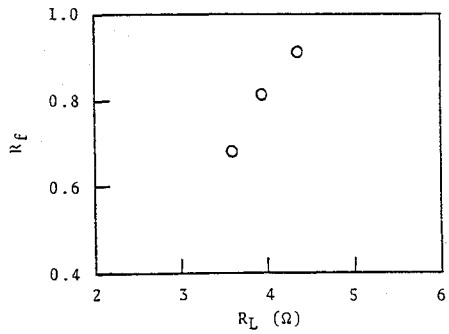

Fig. 10 Relation of load resistance to recovery factor.

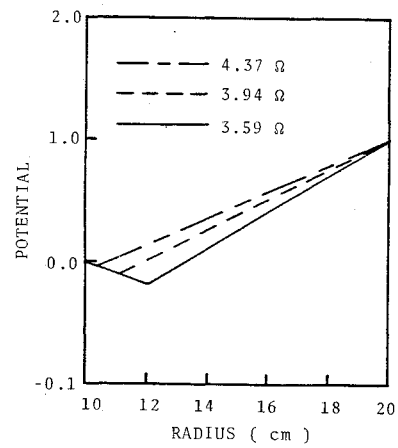

Fig. 11 Potential distribution averaged over the tangential direction for three kinds of load resistance.

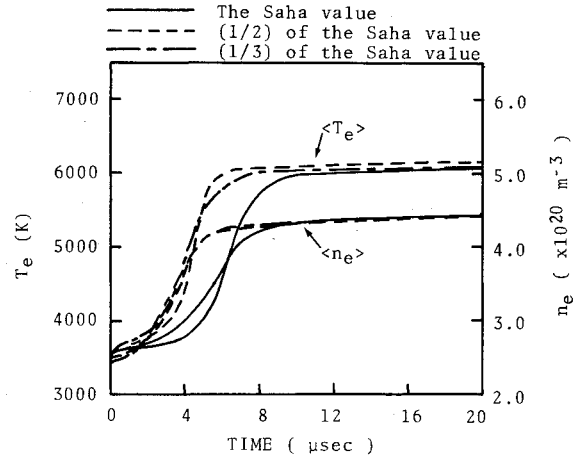

Fig. 12 Evolution of $\langle T_e \rangle$ and $\langle n_e \rangle$ with time for three kinds of inlet electron number density (at 20 μs, $R_L = 0.78\Omega$).

Table 2 Plasma parameters for investigating the effect of the change in the inlet electron number density

Inert gas	Seed	Stagnant pressure, atm	Stagnant temperature, K	Seed fraction, $\times 10^{-5}$	Mach number	Magnetic field strength, T	Load resistance, Ω	Inlet n_e, × the Saha equilibrium value
Ar	K	6	2000	6.0	1.7	3.5	0.78	1
Ar	K	6	2000	6.0	1.7	3.5	0.78	1/2
Ar	K	6	2000	6.0	1.7	3.5	0.78	1/3

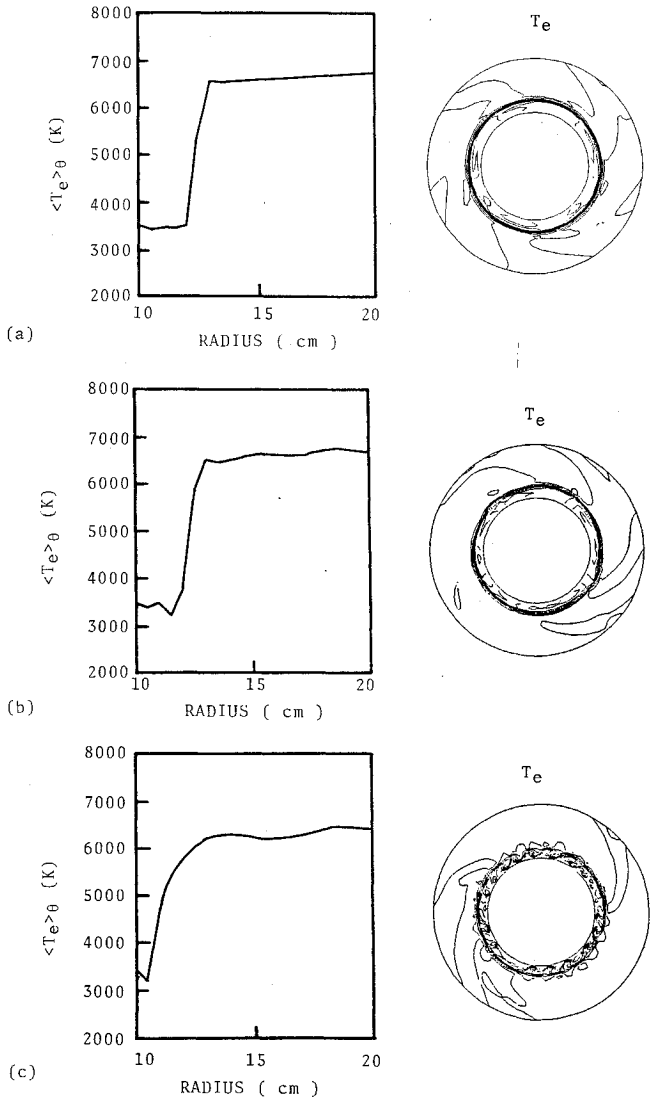

Fig. 13 Distribution of the T_e averaged over the tangential direction (left-hand side) and the isothermal patterns of T_e (right-hand side) for a) n_{ei} = the Saha equilibrium value, b) n_{ei} = one-half of the Saha equilibrium value, and c) n_{ei} = one-third of the Saha equilibrium value (at 20 μs, $R_L = 0.78\Omega$).

Fig. 10, where σ_{eff} and σ_{ideal} are defined as

$$\sigma_{\text{eff}} = \langle j \rangle \cdot \langle j \rangle / \langle j \rangle \cdot \langle E \rangle, \quad \sigma_{\text{ideal}} = e^2 n_e / m_e \nu_e$$

It can be seen in Fig. 10 that we have to keep the relaxation region narrower to achieve a better recovery factor of the electrical conductivity.

From the above numerical analysis, the following conclusion can be drawn: when the gas conditions, the seed fraction, and the magnetic field strength are kept the same, the uniformity of plasma becomes better with the increment of the load resistance, using the concept of fully ionized seed and, as a result, the performance of the generator is expected to be improved.

The distribution of the potential averaged over the tangential direction is plotted along the radial direction as shown in Fig. 11. At the region near the anode the small electrical conductivity causes the potential drop. As T_e and n_e increase in the downstream, the potential tends to recover. This potential profile resembles the experimental results with the shock tunnel.[3,4] It can be found that one can experimentally estimate the relaxation width from the potential profile.

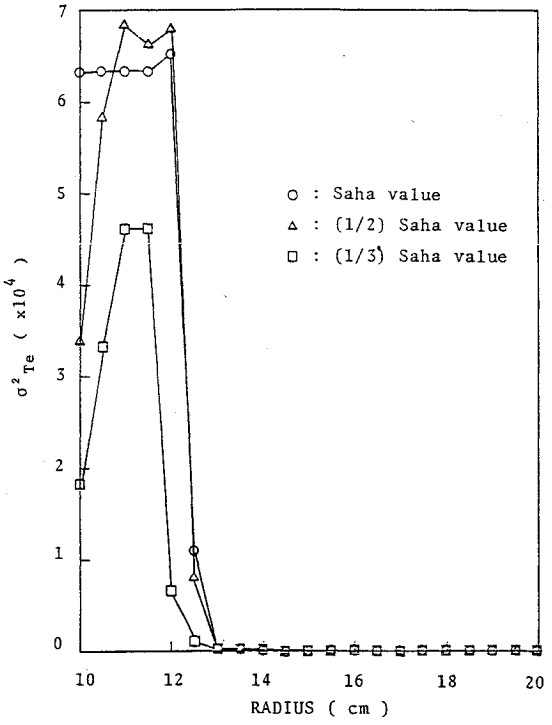

Fig. 14 The variance in the distribution of T_e for a constant radius in the θ direction for three kinds of inlet electron number density (at 20 μs, $R_L = 0.78\Omega$).

Dependence on the Inlet Boundary Condition

In the preceding section the electron temperature of 3500 K and the electron number density equal to the Saha equilibrium value are assumed as the inlet boundary conditions. The inlet boundary conditions generally play an important role in nonlinear numerical analyses, but it is difficult to know the actual values of the inlet electron temperature and the electron number density; therefore, in this section we will study the effect of the change in the inlet electron number density n_{ei}. The inlet electron temperature of 3500 K is again assumed, and three different values of the inlet electron number density are taken; the other conditions, such as working gas, magnetic field, and load resistance, are kept common as listed in Table 2.

Figure 12 shows the evolution of $\langle T_e \rangle$ and $\langle n_e \rangle$ for three different inlet electron number densities. It can be seen from this figure that only a slight change is observed in the evolution profiles of $\langle T_e \rangle$ and $\langle n_e \rangle$ even if the inlet electron number density is changed from the Saha equilibrium value to one-third of the Saha equilibrium value.

On the left-hand side of Fig. 13, the electron temperatures averaged over the tangential direction T_e in the steady state are plotted along the radial direction and, also on the right-hand side, the isothermal patterns of T_e in the steady state are displayed. It is seen that when the inlet electron number density is changed from the Saha value to one-third of the Saha value, the width of the relaxation region remains almost the same, even though the tangentially different electron temperature distributions appear near the inlet.

To compare numerically the widths of the relaxation region, in Fig. 14 we plot the variance of the distribution of the electron temperature in the θ direction defined in Eq. (15). It is found that the change in the inlet electron number density scarcely influences the width of the relaxation region.

Conclusion

It is found from the numerical analyses that the stable state plasma with the fully ionized seed can be dynamically realized

in a channel of the disk-type generator within the framework of our assumptions. The relaxation region is found near the inlet of the channel. In the steady state under the condition of the fully ionized seed, as the load resistance increases, the relaxation region becomes narrower and, as a result, the recovery factor increases so that the performance of the generator is expected to improve. The change of the inlet electron number density has scarcely any influence on the width of the relaxation region, though it affects the tangential structure of the isothermal pattern of T_e in the relaxation region.

References

[1]Nakamura, T. and Riedmüller, W., "Stability of Nonequilibrium MHD Plasma in the Regime of Fully Ionized Seed," *AIAA Journal*, Vol. 12, May 1974, pp. 661-668.

[2]Shioda, S. and Yamasaki, H., "Experimental Studies of Linear MHD Generator with Fully Ionized Seed," *Journal of Energy*, Vol. 2, Nov. 1978, pp. 337-341.

[3]Shioda, S., Yamasaki, H., Matsutani, K., and Sato, H., "Experimental Studies on an Inert Gas Disk Generator with a Small Seed Fraction," *Proceedings of the 18th Symposium on Engineering Aspects of MHD,* 1978, pp. d.2.6.1-d.2.6.7.

[4]Shioda, S., Yamasaki, H., Abe, T., Dahiya, R. P., Saito, S., and Shimazu, Y., "Power Generation Experiments and Prospects of Closed Cycle MHD with Fully Ionized Seed," *Proceedings of the 7th International Conference on MHD,* Vol. 2, 1980, pp. 685-695.

[5]Yamasaki, H. et al., "Effect of Impurities and Gas Temperature on Closed Cycle MHD Generator with Fully Ionized Seed," *Proceedings of the 19th Symposium on Engineering Aspects of MHD,* 1981, pp. 7.4.1-7.4.5.

[6]Abe, T., Kabashima, S., Yamasaki, H., and Shioda, S., "Theoretical Studies on Closed Cycle MHD Generator with Fully Ionized Seed," *Proceedings of the 19th Symposium on Engineering Aspects of MHD,* 1981, pp. 7.5.1-7.5.6.

[7]Abe, T., Kabashima, S., Yamasaki, H., and Shioda, S., "Numerical Studies of a High Interaction MHD Generator with Fully Ionized Seed," *Energy Conversion Management,* Vol. 22, 1982, pp. 251-261.

[8]Rosa, R. J., *Magnetohydrodynamic Energy Conversion*, McGraw-Hill, New York, 1963, Chap. 5.

[9]Mitchner, M. and Kruger, C. H., *Partially Ionized Gases,* John Wiley & Sons, New York, 1973, Chap. 5.

[10]Hara, T., Veefkind, A., and Rietjens, L. H. T., "Numerical Simulation of the Inhomogeneous Discharge Structure in Noble Gas MHD Generators," *AIAA Journal*, Vol. 20, Nov. 1982, pp. 1473-1480.

[11]Harada, N. et al., "Experimental Studies on the Performance of Closed Cycle MHD Generators with Fully Ionized Seed," *Proceedings of the 22nd Symposium on Engineering Aspects of MHD,* 1984, pp. 3.1.1-3.1.14.